Plant Molecular Biology (2005) 59:965–979
DOI 10.1007/s11103-005-2416-7

Laser capture microdissection (LCM) and expression analyses of *Glycine max* (soybean) syncytium containing root regions formed by the plant pathogen *Heterodera glycines* (soybean cyst nematode)

Vincent P. Klink*, Nadim Alkharouf, Margaret MacDonald and Benjamin Matthews
*United States Department of Agriculture, 10300, Baltimore Ave., Bldg. 006, Rm. 118, Beltsville, MD 20705-2350, USA (*author for correspondence; e-mail heartwood27@hotmail.com)*

Received 26 February 2005; accepted in revised form 22 August 2005

Key words: aquaporin, *Glycine max*, *Heterodera glycines* (SCN), Laser capture microdissection (LCM), pathogen, plant, soybean, tubulin

Abstract

Roots of soybean, *Glycine max* cv. Kent L. Merr., plants susceptible to the soybean cyst nematode (SCN), *Heterodera glycines* Ichinohe, were inoculated and allowed to develop feeding sites (syncytia) for 8 days. Root samples enriched in syncytial cells were collected using laser capture microdissection (LCM). RNA was extracted and used to make a cDNA library and expressed sequence tags (ESTs) were produced and used for a Gene Ontology (GO) analysis. RT-PCR results indicated enhanced expression of an aquaporin (GmPIP2,2), α-tubulin (GmTubA1), β-tubulin (GmTubB4) and several other genes in syncytium-enriched samples as compared to samples extracted from whole roots. While RT-PCR data showed increased transcript levels of GmPIP2,2 from LCM tissue enriched in syncytial cells, *in situ* hybridization showed prominent GmPIP2,2 hybridization to RNA in the parenchymal cells tightly juxtaposed to the syncytium. Immunolocalization indicated stronger α-tubulin signal within the syncytium as compared to surrounding tissue. However, α-tubulin labeling appeared diffuse or clumped. Thus, LCM allowed for the isolation of tissue enriched for syncytial cells, providing material suitable for a variety of molecular analyses.

Introduction

The soybean cyst nematode (SCN), *Heterodera glycines* Ichinohe, is an obligate, sedentary endoparasite that is the major pathogen of soybean (*Glycine max*, L. Merr.) and accounts for an estimated 1 billion dollars in production losses annually in the U.S. (Wrather *et al.*, 2001). During parasitism, the SCN penetrates roots and migrates toward the vascular tissue, selects a pericycle or endodermal cell, and initiates the formation of a feeding cell. The nematode induces a variety of changes in the cell it selects for its feeding site. After 1 day, cellular hypertrophy occurs and cell walls dissolve (Endo, 1964). By 42 h, cell wall perforations are observed (Gipson *et al.*, 1971) and cytoplasm from adjoining pericycle, endodermal and cortex cells merges to form a syncytium, a structure that nourishes the SCN during its sedentary and reproductive phases of its life cycle. The syncytium is very different, cytologically, from the root cells it originates and undergoes a variety of changes as it differentiates and becomes the feeding site of the SCN (Endo, 1964, 1965, 1971; Gipson *et al.*, 1971; Jones and Northcote, 1972). The cytoplasm of the developing syncytium appears dense with numerous plastids and ER-like material accumulating (Gipson *et al.*, 1971). Concomitantly, the large vacuole that is present in the cell prior to feeding site selection becomes

reduced in size (Gipson *et al*., 1971). By 7 days, the syncytium has very few small vacuoles with the most obvious cytoplasmic change being the increase in membranous material. Nuclei within the syncytium may (Endo, 1964) or may not (Gipson *et al*., 1971) clump together and as cell walls continue to dissolve, the syncytium expands in size.

While much is known about the cytological aspects of syncytium formation, their molecular analysis has been mired in the inability to physically isolate them from the unwanted tissue that contains them. Laser capture microdissection (LCM) (Isenberg *et al*., 1976; Emmert-Buck *et al*., 1996) offers an approach for obtaining these cells. LCM has been used to study gene expression changes in cells buried in complex tissues or organs (Chiang and Melton, 2003). LCM has been shown to be useful for isolating normal plant tissue (Asano *et al*., 2002), making gene expression comparisons between different tissues in *Zea mays* (Nakazano *et al*., 2003), for obtaining RNA from diverse plant species (Kerk et al, 2003) and even isolating chloroplasts (Meimberg *et al*. (2003). The isolation by LCM of giant cells (GCs) formed during the interaction of the root knot nematode *Meloidogyne javanica* on *Lycopersicon esculentum* was presented (Ramsay *et al*., 2004). This study showed that reverse transcriptase PCR could be used to amplify fragments of four previously characterized genes; two cyclin D genes (LeCyc3;2 and LeCyc3;3), MAPK and actin from GCs isolated and pooled from a wide range of time-points (4–10 days post-inoculation) (Ramsay *et al*., 2004).

Fundamental differences exist between the development of syncytia and GCs (Gheysen and Fenoll, 2002). Those differences make the isolation of syncytia by LCM relevant not only to efforts of studying the SCN infection process, but should translate to other syncytium-forming nematodes and plant cells in general. LCM offered precise microdissection of tissues enriched for syncytia, thus yielding starting material different from our previous studies (Alkharouf *et al*., 2004; Khan *et al*., 2004). We identified many genes, providing a new and more in-depth look at syncytial cells. Increases in transcript levels of some of these genes were confirmed by real time PCR (RT-PCR) with supporting evidence provided by RNA *in situ* hybridization, or antibody localization.

Materials and methods

Nematode and plant preparation

Nematode culture was performed according to Alkharouf *et al*. (2004). Nematode infection was determined by acid fuchsin staining (Byrd *et al*., 1983) at the end of the experiment. Stereomicroscopy was performed with a Nikon SMZ 1500 stereomicroscope (Nikon Corporation, Tokyo, Japan). Images were captured with an Optronics MagnaFire model S99802 CCD camera (Optronics, Goleta, CA).

Tissue procurement

Tissue fixation in Farmer's solution (FS) composed of 75% ethanol, 25% acetic acid (Sass, 1958, Kerk *et al*., 2003) provided superior quality RNA extracted from samples obtained by LCM. In parallel, for *in situ* hybridization and immunohistology, tissue was killed and fixed in 3.7% paraformaldehyde (PFA) buffered with PEMP buffer (100 μM Pipes, 1 μM $MgCl_2$, 1 μM EGTA and 4% polyethylene glycol MW 8000, pH 6.8 (Sugimoto *et al*., 2000) to preserve microtubules. Soybean root tissue was harvested 6 and 8 days after nematode inoculation, while uninoculated roots served as controls. The root tissue was cut into 0.5 cm pieces and vacuum-infiltrated with either FS or PFA at room temperature for 1 h. Fresh fixative (FS or PFA) was added to both samples. Tissue was subjected to an incubation step of 12 h at 4 °C. PFA-fixed tissue was dehydrated through 10, 25, 50, 75% ethanol with the remaining procedure done identically as was done for the tissue processed in FS. The fixative was removed, and roots were dehydrated with a graded ethanol series (75%, 85%, 100%, 100%), 30 min each. Ethanol was replaced with 1:1 xylene:ethanol for 30 min, followed by three, 100% xylene incubations (30 min each). Xylene was then replaced with paraffin by placing the specimens into a 58 °C oven and infiltrating the roots sequentially in 25, 50 and 75% (1×) and 100% (3×) Paraplast + tissue embedding medium (Tyco Healthcare Group LP, Mansfield, MA.) in each step for 3 h. Tissue was cast and mounted for sectioning. Serial sections of roots were made on an American Optical 820 microtome (American Optical Co., Buffalo, NY) at a section thickness of

10 μm. Serial sections were placed onto a pool of dH_2O made RNAse-free with diethyl pyrocarbonate (DEPC) (Sigma, St. Louis, MO) on baked RNAse-free slides without any adhesives. Excess DEPC dH_2O was blotted-off and slides were allowed to dry. Immediately prior to laser capture, slides were dipped in 100% xylene for 5 min followed by a 1:1 xylene:ETOH and 100% ETOH (1 min each) treatment and air-dried.

LCM and syncytium volume estimates

Syncytium region area measurements were made with the Spot 2.2 software package (Diagnostic Instruments, Sterling Heights, MI). Area was calculated by counting the number of pixels in the bound area, inclusive of the pixels on the line drawn. Volume estimations were obtained by multiplying the syncytium-enriched area measurements by the section thickness (10 μm). The volume approximations of each syncytium were calculated as the sum of the regional volumes generated from all 10 μm serial sections of a particular syncytium. Calculations were performed in Microsoft Excel (Microsoft Inc., Seattle, WA). Both LCM and archival image capture of microdissected control tissue and nematode infected roots were performed on the Arcturus PixCell II laser capture microscope (Arcturus Bioscience Inc. Mountain View, CA) with a laser spot size of 7.5 μm. The laser duration was of 100 mV for 3.0 ms. Syncytium-enriched tissue was lifted from the slides onto CapSure^{TM} high sensitivity (HS) cap LCM transfer film (Arcturus) according to the manufacturer's instructions.

RNA extraction and quality assessment

RNA samples were obtained at various stages of the fixation protocol to assess RNA quality. Tissue was ground with a micropestle in 40 μl RNA extraction buffer (Arcturus). A DNAse step was included in these RNA extraction procedures, using DNAfree (Ambion, Austin, TX). Syncytium-enriched tissue from the LCM lifts was washed-off of the HS cap by micropipetting 20 μl of XB buffer (Arcturus) onto the HS cap, and moving the solution to a 1.5 ml microfuge tube. The RNA was extracted and processed with the PicoPure RNA Isolation Kit (Arcturus) according to the manufacturer's instructions, with the addition of a DNAse treatment using DNA-free (Ambion), just before the second column wash. RNA quality and yield were tested according to the RNA 6000 Pico Assay (Agilent Technologies, Palo Alto, CA) on the Agilent 2100 Bioanalyzer according to the manufacturer's instructions.

cDNA library construction of RNA extracted from syncytium-enriched tissue

LCM caps with microdissected tissue that was enriched for syncytia were prepared for RNA extraction. RNA was eluted from the HS LCM cap into 11 μl of elution buffer (Ambion), and 10 μl of this was amplified using the RiboAmp RNA Amplification Kit (Arcturus) according to the manufacturer's instructions. The first strand cDNA was synthesized using a poly A primer with a T7 promoter. Second strand cDNA synthesis was primed with exogenous primers (Arcturus). Amplified RNA (aRNA) was produced using a T7 RNA polymerase. The aRNA was subsequently converted to double stranded cDNA (dscDNA). After being A-tailed with Recombinant Taq Polymerase (Invitrogen, Carlsbad, CA), the cDNA was cloned into pCR4-TOPO vector using the TOPO TA Cloning Kit for Sequencing (Invitrogen). DNA was transformed into One Shot TOP10 electrocompetent cells (Invitrogen) and plated on LB plates with 50 mg/l kanamycin, containing IPTG and X-gal for blue/white bacterial colony selection. White colonies were picked and replicated in 96 well plates. An aliquot (5 μl) of each colony was heat-lysed and PCR-amplified using M13 forward (5′GTAAAACGACGGCCAGT3′) and M13 reverse (5′AACAGCTATGACCATG3′) primers (Qiagen, Valencia, CA). DNA sequencing reactions were conducted with T3 (5′ATTA-ACCCTCACTAAAG3′) and T7 (5′AATACG-ACTCACTATAG3′) primers (Qiagen) using the ABI Prism Big Dye Terminator Cycle Sequencing Ready Reaction Kit (Applied Biosystems, Foster City, CA). DNA sequencing of LCM clones was performed using an ABI Prism 3100 Genetic Analyzer (Applied Biosystems) (Matthews *et al.*, 2004). High quality sequence reads were discriminated using PHRED (Ewing *et al.*, 1998). A second aliquot of RNA was converted directly to cDNA using the iScript cDNA conversion kit

according to the manufacturer's instructions (Bio-Rad, Hercules, CA).

Gene ontology analyses

The EST sequence data for this article have been deposited with the EMBL/GenBank data libraries under accession numbers CN655731-CN656531. The complete gene sequences for α-tubulin (GmTubA1), β-tubulin (GmTubB4) and aquaporin (GmPIP2,2), have been deposited in EMBL/GenBank, Accession Numbers AY907702, AY907703, AY907701, respectively. The GmTubA1, GmTubB4 and GmPIP2,2 nucletotide and deduced protein sequences were analyzed using the DNASTAR analysis software (DNASTAR, Inc., Madison, WI). The ESTs containing overlapping identical sequences were assembled into tentative consensus sequences referred to here as unigenes. Unigenes were queried manually through GenBank using blastn, blastx, tblastn, tblastx, blastp, rpsblast (Altschul *et al*., 1997). The highest blast matches are presented in Table 1 as the Blast-term. Unigenes were queried manually through the Gene Ontology Database (The Gene Ontology Consortium, 2004). The highest GO match is presented in Table 1 as the GO-term with its corresponding GO identification number.

RNA amplification

The RNA amplification protocol was adapted from Iscove *et al*. (2002). The final concentrations of reagents for five μl cDNA synthesis reactions of LCM RNA were: 50 pg of LCM RNA, 1× 1st strand buffer (Invitrogen), 0.5% (v/v) NP-40, 1.0 mM DTT, 0.1 μg acetylated BSA, 5.25 units of RNAguard (Amersham), 10 μM dNTPs (Amersham), RNaseFree Ultra pure dH_2O to 5 μl, 100 units SuperScript III (Invitrogen), 17.6 nM Oligo dT Primer (GTTACCTCGAGAATTCT$_{24}$), 1× tailing buffer (25 mM Tris HCl pH 6.6, 200 mM potassium cacodylate, 1.5 mM $CoCl_2$, BSA 0.25 mg/ml, 0.75 mM dATP) and 200 units of terminal transferase (Roche). The thermocycling reaction was engaged at 65 °C for 90 s. The thermocycler was paused to add the SuperScript III and oligo dT primer. The reaction resumed at 50 °C for 15 min and 20 s, followed by 70 °C for 10 min. The reaction then was paused to add the RNaseH (Invitrogen). The reaction resumed at 37 °C for 15 min and 30 s. The reaction then was paused to add 200 units of terminal transferase and 1X tailing buffer. The reaction resumed at 37 °C for 15 min and 30 s, followed by 65 °C for 10 min and 30 s. The reaction proceeded at 65 °C for 90 s and was subsequently terminated. The cDNA then was amplified for two cycles. The final concentrations of reagents used in the first round of the 20-μl exponential amplification reactions were: 1× HotStarTaq buffer (Qiagen), 10 μM dNTPs, 0.6 μM SR-T24 primer, 0.05 U/μl HotStarTaq (Qiagen), single-stranded cDNA. Thermocycler amplification occurred for 30 cycles. Pre-amplification occurred at 95 °C for 15 min 30 s, 50 °C for 2 min, 72 °C for 2 min. Amplification of the first cycle occurred at 94 °C for 2 min, 60 °C for 15 s, 72 °C for 2 min (repeating the amplification steps 29 more times). The reaction was then held indefinitely at 10 °C. For the second round of amplification, the final concentrations of reagents used in the 20-μl exponential amplification reactions were: 1× HotStarTaq buffer, 10 μM dNTPs, 0.6 μM SR-T24 primer, 0.05U/μl Hot Star Taq, single stranded cDNA. Thirty-five cycles of thermocycler amplification occurred. Pre-amplification occurred at 95 °C for 15 min 30 s, 50 °C for 2 min, 72 °C for 2 min. Amplification of cycle one occurred at 94 °C for 15 s, annealing at 60 °C for 30 s, amplification at 72 °C for 2 min (repeating the amplification steps 34 more times) and then held indefinitely at 10 °C.

RT-PCR of LCM derived clones

Unamplified whole infected root RNA was converted to cDNA using SuperScript First Strand Synthesis System for RT-PCR (Invitrogen) using an oligo d(T) as a primer according to the manufacturer's instructions. RNA from separate isolation events was amplified from both whole infected root and LCM-derived tissue enriched for syncytia and converted to cDNA as previously described (see RNA amplification procedure in the previous section). Independent RNA samples for the different replicate experiments were obtained by LCM from different roots from different individual plants. Replicate experiments were performed in triplicate. RT-PCR was performed using primers found in Table 2. Relative quantities of gene expression

Table 1. ESTs isolated from a cDNA library created from LCM-derived syncytia.

Unigene	Genbank-Term	Go-Term	GO ID
U 17	ribosomal protein S19	structural constituent of ribosome	GO:0003735
U 30	ribosomal protein L11	structural constituent of ribosome	GO:0003735
U 81	ribosomal protein L31	structural constituent of ribosome	GO:0003735
U 84	ribosomal protein S21	structural constituent of ribosome	GO:0003735
U 169	ribosomal protein S26	structural constituent of ribosome	GO:0003735
U 197	ribosomal protein S11	structural constituent of ribosome	GO:0003735
U 8	extensin	glycoprotein network	GO:0048222
U 9	extensin	glycoprotein network	GO:0048222
U 183	extensin	glycoprotein network	GO:0048222
U 189	extensin	glycoprotein network	GO:0048222
U 32	BEL 1 homeodomain	DNA binding	GO:0003677
U 54	G-Box binding protein B12D	DNA binding	GO:0003677
U 106	DNA binding protein p24	DNA binding	GO:0003677
U 144	MYB-related protein	DNA binding	GO:0003677
U 20	sec14	membrane	GO:0016020
U 99	sec13	membrane	GO:0016020
U 139	AtVAMP727	membrane	GO:0016020
U 161	GmDREB1 (AP2-like)	transcription factor activity	GO:0003700
U 179	transcription factor	transcription factor activity	GO:0003700
U 10	ubiquitin	protein ubiquitination during ubiquitin-dependent protein catabolism	GO:0042787
U 11	ubiquitin	protein ubiquitination during ubiquitin-dependent protein catabolism	GO:0042787
U 28	protein kinase (Cf-9)	protein kinase cascade	GO:0007243
U 82	kinase	protein kinase cascade	GO:0007243
U 13	metallothionein	metal ion binding	GO:0046872
U 156	metallothionein	metal ion binding	GO:0046872
U 201	α-tubulin	alpha-tubulin folding	GO:0007024
U 102	β-tubulin	beta-tubulin folding	GO:0007025
U 18	pathogen resistance (SRG2)	defense response to pathogen, incompatible interaction	GO:0009814
U 21	asparaginyl endopeptidase (VmPE-1)	asparaginyl-tRNA aminoacylation	GO:0006421
U 22	lipid-associated	acetyl-CoA metabolism	GO:0006084
U 24	peroxidase	peroxidase-heme linkage	GO:0018186
U 25	small nuclear ribonuclearprotein E	snRNA transcription	GO:0009301
U 29	mitochondrial substrate carrier	mitochondrial transport	GO:0006839
U 35	GH3-like	auxin mediated signalling pathway	GO:0009734
U 37	cytochrome C reductase complex	mitochondrial electron transport, cytochrome *c* to oxygen	GO:0006123
U 38	adenosylhomocysteinase	adenosylhomocysteinase activity	GO:0004013
U 39	UDP-D-apiose/UDP-D-xylose synthase	1,4-beta-D-xylan synthase activity	GO:0047517
U 42	auxin/aluminum-responsive protein	response to aluminum ion	GO:0010044
U 50	dirigent protein	guiding stereospecific synthesis activity	GO:0042349
U 51	seed specific (Bn15D1B)	seed development	GO:0048316
U 52	DNA binding protein	regulation of DNA binding	GO:0051101
U 53	putative quinone oxidoreductase	oxidoreductase activity, acting on NADH or NADPH, quinone or similar compound as acceptor	GO:0016655
U 62	ubiquinol-cytochrome C reductase	cytochrome bc(1) complex assembly	GO:0017062
U 66	28 kDa vegetative storage protein	fat body storage protein uptake	GO:0015032
U 68	translationally-controlled tumor protein	melanotic tumor response	GO:0006969
U 72	ERD15	interacting selectively with an RNA molecule or a portion thereof	GO:0003723
U 74	ferredoxin-thioredoxin reductase	thioredoxin-disulfide reductase activity	GO:0004791
U 80	histone H3	H3/H4 histone acetyltransferase activity	GO:0004406
U 83	ADP-ribosylation factor	ADP-ribosylation factor binding	GO:0030306
U 85	ripening-related protein	ripening, non-climacteric	GO:0009837
U 86	iron–sulfur cofactor synthesis protein	cofactor biosynthesis	GO:0051188
U 90	pre-pro-cysteine proteinase	cysteine catabolism	GO:0009093

Table 1. Continued.

Unigene	Genbank-Term	Go-Term	GO ID
U 94	glycine-rich RNA-binding protein	positive regulation of sterol regulatory element binding-protein target gene transcription	GO:0035104
U 95	DNA-binding enhancer protein	transcription regulator activity	GO:0030528
U 97	cytosolic chaperonin, delta-subunit	chaperonin-mediated tubulin folding	GO:0007022
U 104	NADH dehydrogenase subunit 4L	NADH dehydrogenase activity	GO:0003954
U 105	GDA2	hypersensitive response	GO:0008150
U 119	gibberillin response modulator (RGAI)	response to gibberillic acid stimulus	GO:0009739
U 130	glycogen synthase kinase 3 (GSK-3)	glycogen synthase kinase 3 activity	GO:0004696
U 142	Bor1	boron transporter activity	GO:0046715
U 149	splicing factor 3B	splicing factor protein-nucleus import	GO:0035048
U 151	GTP-binding	metabotropic glutamate receptor signaling pathway	GO:0007216
U 152	abscissic acid ripening induced	response to abscisic acid stimulus	GO:0009737
U 154	small nuclear ribonucleoprotein D	ribonucleoprotein	GO:0003733
U 163	potassium transporter-like [KUP3p]	potassium ion transporter activity	GO:0015079
U 165	seed storage/lipid transfer protein	nutrient reservoir activity	GO:0045735
U 167	glutathione peroxidase	glutathione peroxidase activity	GO:0004602
U 168	elongation factor 1-alpha	peptidyl-diphthamide biosynthesis from peptidyl-histidine	GO:0017183
U 171	cytidine deaminase	cytidine deaminase activity	GO:0004126
U 172	glutaminyl-tRNA synthetase	glutaminyl-tRNA synthase (glutamine-hydrolyzing) activity	GO:0050567
U 188	proline-rich spliceosome-associated	elastin	GO:0001528
U 191	hydroxyproline-rich glycoprotein	4-hydroxyproline biosynthesis	GO:0019472
U 195	carbonic anhydrase	carbonate dehydratase activity	GO:0004089
U 196	LTP family protein	wide spectrum protease inhibitor activity	GO:0017114
U 202	PIP2,2	water channel activity	GO:0015250

Table 2. PCR primer pairs used for RT-PCR. The number in parentheses beside each gene denotes the amplicon length in base pairs.

α-tubulin (54)	U152 (68)
forward 5′TTCTCCATTATTCAAACTGT	forward 5′ATTCAAGCTCCAAAGTATCACCAT
reverse 5′CACCAAAATAGAAGCATAAT	reverse 5′CAAAGGCACACTAGAAATG GAAGA
β-tubulin (56)	U84 (168)
forward 5′AAATAGGGGGTTA GTGGGAGTGG	forward 5′CTAAGATGCAGAACGAGGAAGG
reverse 5′CAGATAGGTGCCGCATAACATTG	reverse 5′GAGAGCAAAAGTGGAGAAATGG
Aquaporin (80)	U18 (52)
forward 5′GTCACCCAAAACAAGAACAGT	forward 5′AAACCGACACTTGCTCAC
reverse 5′CCC ACGGGTAAGCAGAA	reverse 5′CTTGCGGCTTTGTTTG
U72 (93)	U25 (142)
forward 5′AAGGCCCCTAAGTTTGTGAAG	forward 5′ACGGGGAAATGATTAACACTCTG
reverse 5′CTGGTGGTGCTGGGGGAATGG	reverse 5′CATGATAATATTTCTCCCACAACA
U114 (73)	U11 (63)
forward 5′TGTCTTATTGTGGCCTTCTTTAT	forward 5′GACCCTCGCTGACTACAACATC
reverse 5′GTTGCAGCTTACATCACGA	reverse 5′CCACGGAGACGGAGGACA
U37 (75)	U130 (145)
forward 5′TAGCCCCCAATAATGTG	forward 5′TGTTCTTCAGCCTCTTCT
reverse 5′GAAAACGCTCAAACTCAGA	reverse 5′GGCTTGCAACCCTATCAC

were determined using the Stratagene M×3000P Real-Time PCR system (Stratagene, La Jolla, CA) using the manufacturer's instructions. DNA accumulation during the reaction was measured with SYBR Green with ROX as the reference dye. RT-PCR of genes was performed with serial dilutions over a four-log range. PCR efficiencies were equal. The C_t values and relative abundances from our experiments were calculated using software supplied with the Stratagene M×3000P Real-Time PCR system. Data analysis was performed according to the $2^{-\Delta\Delta C}$t method

(Livak and Schmittgen, 2001) using unamplified infected root RNA as the calibrator sample with the ribosomal gene S21 as the internal control gene. Controls for RT-PCR had included reactions containing either no template or RNA processed with no Superscript reverse transcriptase. Both the SYBR Green dissociation curve of amplified products and gel electrophoresis demonstrated the production of only one product per reaction. DNA for the RT-PCR was dissociated for 10 min at 96 °C, followed by PCR cycling and temperatures set for denaturation for 30 s at 96 °C, annealing for 60 s at 55 °C and extension for 30 s at 72 °C.

In situ *hybridization*

Riboprobes were generated from DNA templates obtained from the LCM library. The DNA templates were amplified by PCR with T7 and T3 promoter containing primers. The conditions for PCR were: denaturation, 96 °C for 30 s; annealing, 50 °C for 15 s; extension, 60 °C for 4 min (30 cycles) using Platinum Taq Polymerase (Invitrogen). The PCR inserts were gel purified with QIAquick Gel Extraction Kit (Qiagen) according to the manufacturer's instructions. *In vitro* transcriptions were performed with the AmpliScribe T7 and T3 Transcription Kit (Epicentre, Madison, WI) according to the manufacturer's instructions with the exception that digoxigenin-11-UTP (Roche Diagnostics Corporation, Indianapolis, IN) was added. Briefly, 1 μg of DNA template was added to a 10 μl transcription reaction. The reaction consisted of 7.5 mM ATP, CTP, GTP and 0.25 mM dUTP, 2.5 mM digoxigenin-11-UTP (in place of UTP), 10 mM dithiothreitol (DTT), 1× reaction buffer and T3 or T7 polymerase. The reaction proceeded at 37 °C for 3 h. RNA was NH_4OAC precipitated to remove unincorporated nucleotides. The RNA probe was re-suspended according to Long and Barton (1998) in 50% deionized formamide. The RNA probe was denatured at 80 °C for 2 min followed by incubation on ice for 5 min. The riboprobe was used at a concentration of 50–100 ng/slide. The *in situ* hybridization protocol was adapted from Long and Barton (1998). Observations were captured on a Nikon E 800 microscope with the Nikon DXM 1200 digital camera fitted with the Nikon Act-1 computer package.

Immunolabeling

Tissue processed in 3.7% PFA in PEMP buffer and embedded in paraffin was cut into serial sections to 10 μm thickness and dried onto poly-lysine-coated slides. Slides were de-paraffinized for 10 min with xylene, dehydrated through ETOH and then hydrated. The remainder of the labeling procedure was done according to Klink and Wolniak, (2001). The α-tubulin labeling was done with the anti-α-tubulin monoclonal antibody DM1A (Sigma). The α-tubulin antibody DM1A recognizes α-tubulin in wheat (Abdrakhamanova *et al*., 2003) and tobacco (Lee *et al*., 2001) by antibody binding to the conserved epitope (AALEKDYEEVG [aa 426–436]) that is found in all α-tubulins (Breitling and Little, 1986). Primary antibody detection was done with the donkey anti-mouse IgG secondary antibody Alexa Fluor 488 (Molecular Probes Inc., Eugene, OR) diluted 1:500 in PEMPT. Control slides either eliminated the primary antibody (non-specific secondary antibody labeling control) or eliminated the secondary antibody (autofluorescence control). Flutax-2 localization was performed according to Diaz *et al*., (2003). Fluorescence imaging was performed using a Zeiss LSM 410 (Carl Zeiss Inc., Thornwood, NY).

Results

Syncytium establishment by Heterodera glycines nematodes on Glycine max plants

G. max cv. Kent soybean seedlings inoculated with second stage juvenile (J2) soybean cyst nematodes (SCN) and grown for eight days reveal the cytological changes that accompany infection (Endo, 1964, 1965, 1971; Gipson *et al*., 1971; Jones and Northcote, 1972). An abundance of J2s were detected at the vascular cylinder using acid fuchsin staining (Figure 1A, arrow). These nematodes had increased girth compared to the original free-living J2 stage nematodes (data not shown) or nematodes not associated with the vascular cylinder (Figure 1A, arrowhead). Serial sections confirm that syncytia were established (Figure 1B, arrows) from nematodes (Figure 1B, arrowhead).

Important changes in the cytology occur during the development of syncytia. Thus, it was

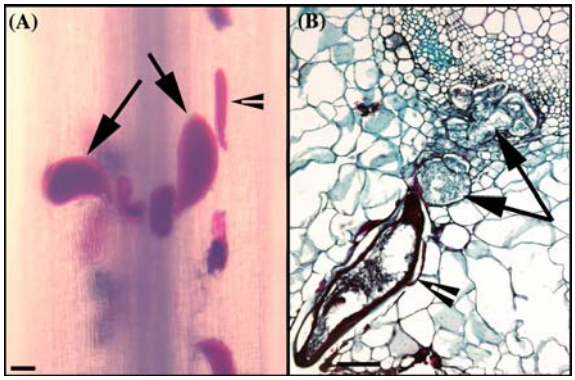

Figure 1. *G. max* cv. Kent seedlings were inoculated with *H. glycines* J2s then grown for 8 days. (A) Acid fuschin staining reveals enlarged nematodes (arrows) at the vascular cylinder. A smaller nematode not associated with the vascular cylinder has also stained (arrowhead) (bar = 500 μm). (B) Transverse section showing the syncytium (arrows) with a closely associated nematode (arrowhead) (bar = 100 μm).

important for our study to isolate syncytia of a homogeneous age. We sought to microdissect syncytia typical of 8-day infected roots. However, root infection by the SCN is not synchronous and syncytia of varying sizes were encountered. Since the syncytium is a chimera, composed of cells originally having different identities (pericycle, endodermis, cortex) that have subsequently merged, we could not rely on cell counts to estimate the age or size of a typical syncytium of a particular timepoint. This complicated the estimation of the number of cells captured for these studies. We, instead, made syncytium volume estimations of LCM tissue obtained from our processed roots. Volumes were estimated on syncytia formed by single nematodes at two different timepoints (6 and 8 days post-inoculation). Syncytia measured at the 6-day timepoint were 768 ± 258 mm^3 ($n = 12$) while syncytia measured at the 8-day timepoint were 1711 ± 655 mm^3 ($n = 9$). These approximations provide a rough estimate of the syncytia volume at those timepoints and show that the syncytia we used were typical of roots infected for 8 days.

SCN-infected root tissue was visually screened for syncytia (Figure 2A, arrow) and syncytium-enriched tissue was isolated using LCM. After LCM the tissue that includes the syncytium is absent in the original sample (Figure 2B, arrow) and present on the collection cap (data not shown).

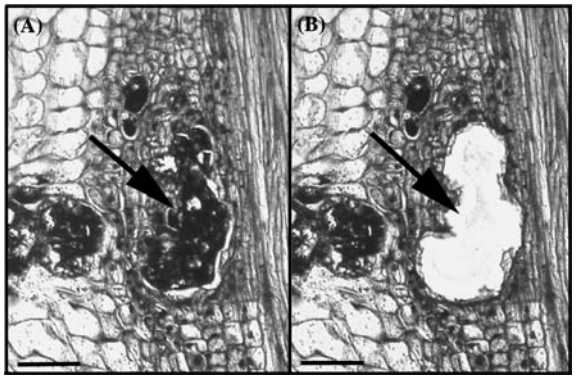

Figure 2. LCM of a syncytium. (A) Depicts a longitudinal section of a root with nematode (arrow) before LCM. (B) Depicts the same section after LCM with the microdissected syncytium region being absent from the section (arrow) (bars = 100 μm).

EST analyses of cDNAs from syncytium-enriched tissue

A cDNA library was constructed with RNA extracted from LCM-derived tissue enriched for syncytia at the 8-day timepoint. Approximately 800 cDNA clones were one-pass sequenced and the resulting expressed sequence tags (ESTs) were assembled into 174 tentative consensus sequences referred to here as unigenes. Only results with positive matches for the Gene Ontology (GO) analysis (The Gene Ontology Consortium, 2004) are presented in Table 1.

Real-Time PCR of specific transcripts in LCM-derived syncytia

Real-time PCR (RT-PCR) experiments were done using primers (Table 2) of genes isolated from LCM-derived tissue enriched for the syncytium. The aim was to identify changes in gene expression of a subset of our unigenes between LCM-derived tissue enriched for the syncytium and whole roots infected with the SCN at the 8-day timepoint. However, the amount of RNA obtained from laser-captured cells is typically limiting. Thus, part of our experiment would involve the use of amplified RNA from limiting amounts of LCM-derived tissue enriched for syncytia. The comparisons that we made were between three sample types: (1) unamplified whole root RNA (2) amplified whole root RNA) and (3) amplified RNA from LCM-derived tissue enriched for syncytia.

We made three sets of comparisons (Figure 3A–C). The first comparison was between unamplified whole root samples and amplified whole root samples (Figure 3A). These experiments showed minimal fold change for all 12 LCM-derived clones (Figure 3A). Thus, it appeared that the amplification process did not affect the RNA. The second comparison was between amplified syncytium RNA and unamplified whole root RNA (Figure 3B). These experiments showed increases for several of our unigenes in the syncytium enriched samples (Figure 3B). These unigenes are: GmTubB4, aquaporin, GmTubA1, unigene 72 (U72), U18 and U114. In this comparison, U11 appeared to experience a decrease in the syncytium-enriched samples meanwhile, U152, U25, U130, U37 and U84 appeared to be relatively unchanged (Figure 3B). The third comparison (Figure 3C) was made between amplified syncytium samples and amplified whole root samples. These experiments (Figure 3C) showed increases for several of our unigenes. These unigenes are: GmTubB4, GmPIP2,2, GmTubA1, U72, U18 and U114. U11 appeared to experience a decrease in the syncytium-enriched samples while U152, U25, U130, U37 and U84 appeared to be unchanged.

Isolation of an aquaporin from LCM-derived syncytia and RNA expression pattern

One gene that showed an increase between samples from LCM-derived samples enriched for the syncytium and whole root samples was an aquaporin gene related to the family of plasma intrinsic proteins (PIP). This aquaporin was isolated from cDNA made from LCM-derived tissue enriched for the syncytium. Sequence analyses revealed this aquaporin is 77.7% identical at the amino acid level to the *Juglans regia* (English walnut) PIP, JrPIP2,2 (Accession Number AAO39008) (Sakr *et al*., 2003) and 74.9% identical at the amino acid level to the *Raphanus sativus* (radish) PIP, RsPAQ2 (Accession Number BAA32778) (Suga *et al*., 2001). We therefore designated this aquaporin *G. max* PIP2,2 (GmPIP2,2) due to its similarity to aquaporins of the PIP2,2 class (Figure 4). The

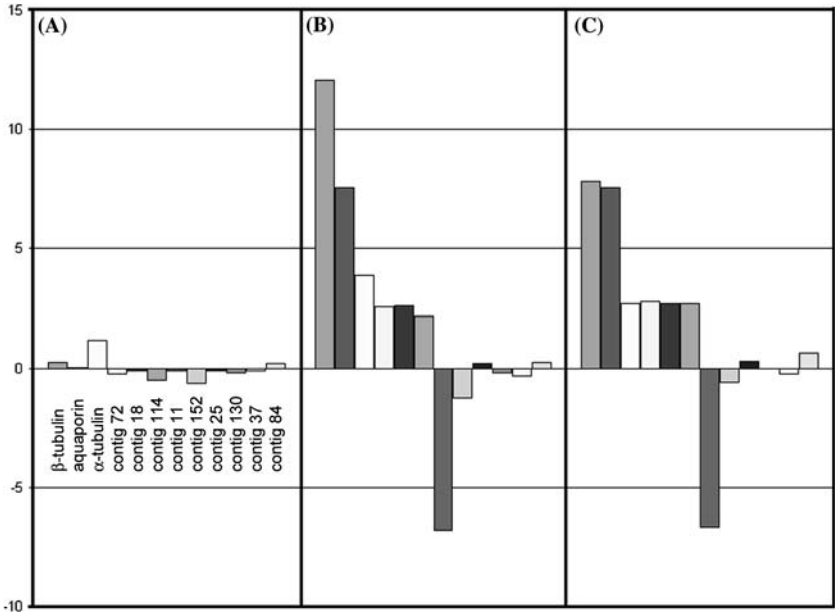

Figure 3. RT-PCR of cDNA clones isolated from LCM-derived tissue enriched for syncytia. The *x*-axis represents the cDNA clones used in the experiment. In each figure, (7A, 7B and 7C), the unigenes studied (left to right) are β-tubulin, aquaporin, α-tubulin, U72, U18, U114, U11, U152, U25, U130, U37 and U84, respectively. The *y*-axis represents the fold difference in expression obtained between the two samples being compared. (A) Comparison of the fold change between unamplified RNA from whole roots infected for 8 days with the SCN and amplified RNA from those same whole roots. (B) Comparison of fold change between amplified RNA from LCM-derived tissues enriched for syncytia with unamplified RNA from whole roots infected for 8 days with the SCN. (C) Comparison of fold change between amplified RNA from LCM-derived tissues enriched for syncytia with amplified RNA from whole roots infected for 8 days with the SCN.

only annotated soybean PIP protein sequence in Genbank is GmPIP1 (accession number T06434) isolated from the cultivar Essex (Maitra and Cushman, 1994). GmPIP2,2 is 76.8% identical to GmPIP1. GmPIP2,2 was used to synthesize sense (control) and antisense digoxigenin-labeled riboprobes for *in situ* hybridization experiments (Figure 5). In our control experiments, *in situ* hybridization using a labeled GmPIP2,2 sense strand riboprobe yielded little background label in the tissue that surrounded the syncytium (Figure 5A). *In situ* hybridization using antisense-labeled GmPIP2,2 probe yielded positive hybridization within the parenchymal cells immediately adjacent to and tightly juxtaposed to the syncytium (Figure 5B). This result was a surprise, especially since the GmPIP2,2 cDNA was isolated from LCM-derived tissue enriched for the syncytium and the microdissections were shown to be specific for the syncytium (Figure 2B). However, even though the LCM was performed on syncytia it does not mean that those genes are excluded from or do not exist in cell or tissue types other than the syncytium. The comparison made in our RT-PCR experiment was between amplified syncytia RNA and whole infected root RNA that should also contain the GmPIP2,2 RNA. We believe that the quantity of RNA from tissues such as the epidermis and cortex that typically do not contain high levels of PIP2,2 aquaporins (Suga *et al*., 2001) may have diluted out the higher levels of GmPIP2,2 RNA observed in the parenchyma cells immediately surrounding the syncytium in the whole infected root samples. Therefore, our comparison of GmPIP2,2 RNA levels between the whole infected roots and the syncytium revealed relatively low levels within the whole root samples. These results point toward the utility of *in situ* hybridization experiments in addition to RT-PCR in understanding the GmPIP2,2 expression pattern. Immunolabeling experiments would contribute further to a better understanding of GmPIP2,2 protein levels and distribution within these cell types.

Analysis of unique tubulin cDNAs and protein expression pattern

Changes in the cytology and increases in the size of syncytia during its development implicated changes in the cytoskeleton may occur during syncytium expansion. Microtubules (MT), composed of dimers of α and β-tubulin, are known to exhibit changes in orientation as a consequence of

```
GmPIP2,2     MAK-DVEQVTEQGEYSAKDYHDPPPAPLIDPDELTKWSLYRAAIAEFIATLLFLYITVLT
JrPIP2,2     MAK-DIE-AAGQGGFSAKDYHDPPPAPLIDAEEFTQWSFYRAIIAEFIATLLFLYITVLT
RsPaq2       MAK-DVE-AVSGEGFQTRDYQDPPPAPLFDPEELTKWSFYRAVIAEFVATLLFLYITVLT
GMPIP1       MAKHDVE----GGSFSAKDYHDPPPAPLIDAEELTQWSFYRALIAEFIATLLFLYITVLT
             *** * *           ** ******* *  * * ** *** **** ************

GmPIP2,2     IIGYKRQSDTKIPGNTECDGVGILGIAWAFGGMIFILVYCTAGISGGHINPAVTFGLFLG
JrPIP2,2     VIGYKSQTD-KAKGGDDCGGVGILGIAWAFGGMIFVLVYCTAGISGGHINPAVTFGLFLA
RsPaq2       VIGYKIETD-STAGGVDCGGVGILGIAWAFGGMIFILVYCTAGISGGHINPAVTFGLLLA
GMPIP1       VIGYKSQSD-VKAGGDVCGGVGILGIAWAFGGMIFILVYCTAGISGGHINPAVTFGLFLA
              ****   *    *   * ***************** ******************** *

GmPIP2,2     RKVSLVRALLYMIAQCAGAICGAGLAKGFQKSFYNRYGGGVNTVSDGYNKGTALGAEIIG
JrPIP2,2     RKVSLVRAVFYMAAQCLGAVCGCGLVKAFQKAYYSKYGGGANELADGYSKGTGLAAEIIG
RsPaq2       RKVSLVRAILYMVAQCLGAICGVGFVKAFQSAYYVRYGGGANSLADGYSTGTGLAAEIIG
GMPIP1       RKVSLIRAIMYMVAQCLGAICGVGLVKAFQKAYYNRYGGGANELSEGYSTGVGLGAEIIG
             ***** **  ** *** ** ** *  * **   *  **** *    **  *  * *****

GmPIP2,2     TFVLVYTVFSATDPKRNARDSHVPVLAPLPIGFAVFMVHLATIPVTGTGINPARSFGPAV
JrPIP2,2     TFVLVYTVFSATDPKRNARDSHVPVLAPLPIGFAVFMVHLATIPITGTGINPARSFGAAV
RsPaq2       TFVLVYTVFSATDPKRSARDSHVPVLAPLPIGFAVFMVHLATIPITGTGINPARSFGAAV
GMPIP1       TSGGVYTVFSATDPKRNARDSHVPVLAPLPIGFAVFMVHLANIPVTGTGINPARSLGAAV
             *   ************ ********************** ** ********** * **

GmPIP2,2     IFNNDKAWDDQWIYWVGPFVGAAVAAIYHQYILRGSAIKALGSFRSNA
JrPIP2,2     IYGKDKAWDDQWIFWVGPFIGAAIAAFYHQYILRAAAAKALGSFRSSS
RsPaq2       IFNESKPWDDHWIFWVGPFIGAAIAAFYHQFVLRASGSKSLGSFRSAANV
GMPIP1       MYNQQKAWDDHWIFWVGPFIGAAIAAFYHQFILRAGAAKALGSFRSNPTI
                  * *** ** ***** *** ** ***  **    * ******
```

Figure 4. Gm PIP2,2 was isolated from LCM-derived syncytium cDNA. The stars below the alignment denote amino acids with perfect matches between the different proteins. The underlined amino acids *NPAVT* at amino acids 109–113 and *NPA* at amino acids 230–232 denote putative extramembrane loops.

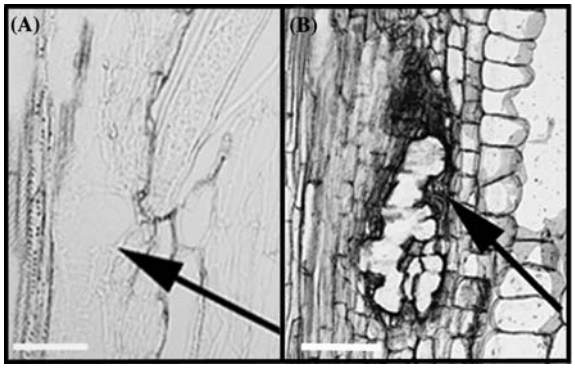

Figure 5. SCN-infected root sections were processed for *in situ* hybridization using digoxigenin-labeled riboprobes derived from the GmPIP2,2 cDNA. (A) Sense-labeled GmPIP2,2 RNA (control) shows minimal background labeling of root tissue surrounding the syncytium (arrow) (bar = 100 μm). (B) Positive GmPIP2,2 hybridization in and around the parenchymal cells that surround the syncytium (arrow) (bar = 100 μm).

plant cell injury (Yuan *et al*., 1994) and drug-induced depolymerization by oryzalin and stabilization of MTs with taxol have yielded cells with increased radial cell expansion much like what was observed in syncytia (Figure 1B). Furthermore, diffuse MT networks have been observed in syncytia using the electron microscope in soybean (Jones and Northcote, 1972). While at the molecular level, immunolabeling with anti-tubulin antibodies and labeling MTs with a green fluorescent protein-labeled microtubule associated protein 4 (GFP-MAP4) have intensely decorated these diffuse MTs in *Arabidopsis thaliana* (de Almeida Engler *et al*., 2004). Unigene analyses revealed numerous unique sequences not present as published annotated genes in GenBank, including those encoding α-tubulin and β-tubulin. Full-length cDNA sequences were obtained for α-tubulin (GmTubA1) that has 97% identity at the amino acid level to alpha-5 tubulin from *A. thaliana* (Accession Number AAA32891) (data not shown). No published DNA sequences encoding *G. max* α-tubulins exist in GenBank.

We explored the protein localization pattern of α-tubulin to better understand the results of the RT-PCR experiments. Commercial α-tubulin antibodies were used here to probe the syncytium for the presence of α-tubulin. The GmTubA1 protein sequence contains a perfectly conserved DM1A antibody recognition motif (AALEKDYEEVG (amino acids 426–436)) that is found in α-tubulin.

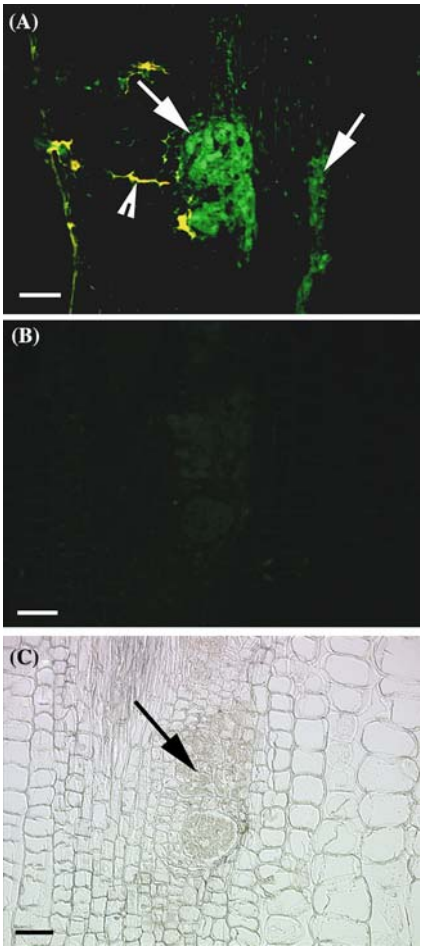

Figure 6. The immunolocalization of α-tubulin in syncytia. (A) A root section shows the syncytium exhibiting α-tubulin immunolabel (arrow, green fluorescence). The yellow autofluorescence (arrowhead) occurs at the damage trail and is caused by the nematode as it burrows through the root and migrates toward the vascular cylinder (bar = 100 μm). (B) A root section yields little background staining when the primary antibody is eliminated from the procedure (bar = 100 μm). (C) The same micrograph as in (B) under brightfield illumination (bar = 100 μm).

Thus, this antibody should recognize the GmTubA1 protein, obviating the concern of using heterologous antibodies for GmTubA1 detection. The α-tubulin antibody strongly labeled the syncytium (Figure 6A, arrows), while the surrounding tissue was only weakly labeled. Control root sections exhibit only weak fluorescence throughout the root section (Figure 6B) with that light micrograph showing the control root section with syncytium (Figure 6C). These data suggest the presence of higher amounts of α-tubulin within the

syncytium than in surrounding cells. These data support previous observations of increased α-tubulin promoter activity (Green *et al*. 2002), however, in giant cells of rice plants formed by *Meloidogyne incognita* and an increase in immunolabeling of α-tubulin protein in the syncytia of *A. thaliana* formed by *Heterodera schachtii* (de Almeida Engler *et al*., 2004).

We also isolated a β-tubulin cDNA (GmTubB4). GmTubB4 is 95.1% identical at the amino acid level to TUBB (Accession Number P28551) isolated from the soybean cultivar Williams (Tonoike *et al*., 1994), 91.5% identical at the amino acid level to the soybean tubulin beta-2 chain (Accession Number P12459) (Guiltinan *et al*., 1987) and 89.4% identical at the amino acid level to the soybean tubulin beta-2 chain (accession number JA0049) (Guiltinan *et al*., 1987) (data not shown). Thus, GmTubB4 is different than other previously isolated β-tubulins from soybean. We explored the protein localization pattern of β-tubulin to better understand the RT-PCR experiments using Flutax-2, a fluorescently labeled taxol analog that binds to microtubules on an epitope of the β-tubulin protein (Rao *et al*., 1995; Diaz *et al*., 2003) (Data not shown). These observations of β-tubulin distribution within the syncytium as revealed by Flutax-2 resemble α-tubulin distribution within syncytia, consistent with the observations of de Almeida Engler *et al*., (2004).

Discussion

The syncytium undergoes a variety of cytological changes as it differentiates and becomes the feeding site of the SCN (Endo, 1964, 1965, 1971; Gipson *et al*., 1971; Jones and Northcote, 1972). From their original observations, it is clear that there are ongoing molecular changes occurring within the syncytium as it differentiates. Studying those changes has been complicated because of the technical limitation of concentrating syncytia cytoplasm as they are embedded within the root. We reduced this complication by isolating tissue enriched for syncytia by LCM. In our work, RNA from LCM-derived tissue enriched for syncytia was used to create a cDNA library for cloning and GO analyses, perform RT-PCR experiments and generate probes for *in situ* hybridization.

Many of our unigenes yielded positive matches in the GO database. However, a majority of the unigenes could not be ascribed any GO annotation. RT-PCR experiments reveal that some of the unigenes experienced little change in expression between LCM-derived tissues enriched for syncytia and the whole root samples. These genes are: U152, an ABA responsive gene; U25, a snRNP-E protein homolog; U130, a glycogen synthase kinase-3 (GSK3) homolog; U37, a cytochrome C reductase complex protein homolog and U84, a ribosomal S21 homolog. We observed that GmTubB4, GmPIP2,2, GmTubA1, U72, an ERD15 homolog; U18, an ABR17 pathogen resistance gene homolog; and U114, a gene of unknown function had experienced increases in the LCM-derived tissue samples enriched in syncytia as compared to both unamplified and amplified whole root samples. U11, an ubiquitin protein homolog exhibited a decrease in LCM-derived tissues enriched for the syncytium. Our knowledge of gene expression using RT-PCR of RNA extracted from LCM-derived tissues enriched for the syncytium has aided our understanding of less understood genes (U72, U18, U114, U152, U25, U130 and U37).

An aquaporin was isolated from our cDNA library that was constructed from RNA extracted from LCM-derived tissue enriched for syncytia. Aquaporins are involved in water transport where different aquaporin gene family members exist in different cell types (Suga *et al*., 2001; Javot and Maurel, 2002; Sakr *et al*., 2003). The LCM-derived aquaporin is most similar to the PIP2,2 plasma intrinsic proteins. Therefore, we designated our *G. max* aquaporin as GmPIP2,2. RT-PCR assays indicated that GmPIP2,2 transcripts are elevated within our syncytium-enriched tissue as compared to whole root SCN-infected mRNA extracts. The *in situ* hybridization with digoxigenin-labeled RNA probes for GmPIP2,2 showed pronounced staining in the parenchyma composing the dense perimeter of cells surrounding the syncytium. This result was surprising since the cDNA was isolated from microdissected syncytia. However, isolating cDNA from specific cell types does not mean that those transcripts are precluded from other cells, tissues or organs. For example, observations were made recently for two cyclin D genes (LeCyc3;2 and LeCyc3;3), MAPK and actin in reverse transcriptase PCR experiments comparing RNA from microdissected GCs and leaves in

Lycopersicon (Ramsay *et al*., 2004). Those experiments revealed LeCyc3;2 and LeCyc3;3, MAPK and actin expression in both GCs and leaves (Ramsay *et al*., 2004). It would be expected that the cells surrounding the syncytium presumably may be involved as a water source for the syncytium and thus would express GmPIP2,2. Immunolabeling with antibodies for GmPIP2,2 would help our understanding of its expression pattern in these cells.

We have found the use of antibody localization useful to corroborate our RT-PCR studies and reveal protein expression patterns of genes previously identified as being expressed in nematode feeding sites. For example, Green *et al*. (2002) demonstrated by GUS (β-glucuronidase) localization that the activity of the *A. thaliania* tubulin-1 promoter was retained in giant cells of rice plants formed by *Meloidogyne incognita*. Tubulin composes MTs, structures involved in a variety of cell processes, including cell wall modification and expansion (Lloyd and Chan, 2004). Our immunolocalization data indicate stronger α-tubulin labeling in soybean syncytial cells formed by SCN than in root cells further from the infection site. Similar observations of MT labeling patterns were made recently for tubulin in the syncytia of *A. thaliana* using both immunolocalization of tubulin and observations of GFP-MAP4 distribution patterns (de Almeida Engler *et al*., 2004). GFP-MAP4 expression in those cells was diffuse (de Almeida Engler *et al*., 2004) and did not exhibit staining typical of MT localization (Marc *et al*., 1998). We cannot reconcile why we have not observed typical MT arrays in these cells. However, MTs are highly sensitive to their intracellular environment and have been shown to be depolymerized in plant cells by calcium, aluminum and glutamate (Sivaguru *et al*., 2003). Tubulin polymerizes into protofilament sheets in the presence of cobolt (Wallin *et al*., 1977) or by binding to zinc (Larsson *et al*., 1976). Several other cations can either stimulate or inhibit tubulin polymerization (Wallin *et al*., 1977; Guskin and Kress, 1977). Maintaining the 1:1 α and β-tubulin stoichiometric ratio in cells is important for normal MT dynamics and cell function as well (Bollag *et al*., 1990; Bhattacharya and Cabral 2004). The strong, but diffuse staining pattern observed for α-tubulin (also revealed by de Almeida Engler *et al*., (2004)) may indicate a physiological property of MTs occurring within syncytia.

A number of other genes reported by others as being expressed in nematode infected roots (See Gheysen and Fenoll (2002) for review) were identified in our cDNA library from syncytium-enriched cells. For example, we identified ESTs that encode extensin and peroxidase. These proteins are expressed in roots infected by nematodes. Van der Eycken et al (1996) identified two extensin genes in tomato giant cells formed by *M. incognita*. Peroxidase is expressed in *A. thaliana* in early interactions with *M. incognita* (Vercauteren *et al*., 2001). Extensin and peroxidase are induced in *G. max* cv. Kent roots infected for two days with the SCN (Khan *et al*., 2004).

As we explore further the expression profiles of these and other cDNAs we are beginning to demonstrate the ability of LCM to enrich for cell types that express those transcripts. Conversely, we can select for cells with decreased levels of a particular transcript. Thus, LCM will be a powerful resource for the study of plant cells that are recalcitrant to their isolation, especially where expression patterns may be masked by the mass of its surrounding tissue.

Acknowledgments

We gratefully acknowledge Joseph Urban, USDA-ARS-BHNRC-NRFL, Beltsville, MD for access to the Arcturus PixCell II laser capture microscope; Theresa Taylor, Arcturus Bioscience, Inc.; Terez Shea-Donohue, USDA-ARS-BHNRC-NRFL, Beltsville, MD and Wesley Garrett, Biotechnology and Germplasm Laboratory, USDA-ARS-ANRI, Beltsville, MD. Dave Straney, University of Maryland, Department of Cell Biology and Molecular Genetics, Leslie Wanner, USDA-ARS-Vegetable Laboratory, Beltsville, MD and Ann Smigocki, USDA-ARS-Molecular Plant Pathology Laboratory, Beltsville, MD for critical review of the manuscript. The authors thank Kristina Pilitt for her expert technical assistance. Mention of trade names or commercial products in this article is solely for the purpose of providing specific information

and does not imply recommendation or endorsement by the United States Department of Agriculture.

References

Abdrakhamanova, A., Wang, Q.Y., Khokhlova, L. and Nick, P. 2003. Is microtubule disassembly a trigger for cold acclimation?. Plant Cell Physiol. 44: 676–686.

Alkharouf, N., Khan, R. and Matthews, B. 2004. Analysis of expressed sequence tags from roots of resistant soybean infected by the soybean cyst nematode. Genome 47: 380–388.

de Almeida Engler, J., Van Poucke, K., Karimi, M., De Groodt, R., Gheysen, G., Engler, G. and Gheysen, G. 2004. Dynamic cytoskeleton rearrangements in giant cells and syncytia of nematode-infected roots. Plant J. 38: 12–26.

Altschul, S.F., Madden, T.L., Schaffer, A.A., Zhang, J., Zhang, Z., Miller, W. and Lipman, D.J. 1997. Gapped BLAST and PSI-BLAST: a new generation of protein database search programs. Nucl. Acids Res. 25: 3389–3402.

Asano, T., Masumura, T., Kusano, H., Kikuchi, S., Kurita, A., Shimada, H. and Kadowaki, K. 2002. Construction of a specialized cDNA library from plant cells isolated by laser capture microdissection: toward comprehensive analysis of the genes expressed in the rice phloem. Plant J. 32: 401–408.

Bhattacharya, R. and Cabral, F. 2004. A ubiquitous beta-tubulin disrupts microtubule assembly and inhibits cell proliferation. Mol. Biol. Cell 15: 3123–3131.

Bollag, D.M., Tornare, I., Stalder, R., Paunier Doret, A.M., Rozycki, M.D. and Edelstein, S.J. 1990. Overexpression of tubulin in yeast: differences in subunit association. Eur. J. Cell Biol. 51: 295–302.

Breitling, F and Little, M 1986. Carboxy-terminal regions on the surface of tubulin and microtubules. Epitope locations of YOL1/34, DM1A and DM1B. J. Mol. Biol. 189: 367–370.

Byrd, D.W. Jr., Kirkpatrick, T. and Barker, K.R. 1983. An improved technique for clearing and staining plant tissue for detection of nematodes. J. Nematol. 15: 142–143.

Chiang, M.K. and Melton, D.A. 2003. Single-cell transcript analysis of pancreas development. Dev. Cell 4: 383–393.

Diaz, J.F., Barasoain, I. and Andreu, J.M. 2003. Fast kinetics of Taxol binding to microtubules. Effects of solution variables and microtubule-associated proteins. J. Biol. Chem. 278: 8407–8419.

Emmert-Buck, M.R., Bonner, R.F., Smith, P.D., Chuaqui, R.F., Zhuang, Z., Goldstein, S.R., Weiss, R.A. and Liotta, L.A. 1996. Laser capture microdissection. Science 274: 998–1001.

Endo, B. 1964. Penetration and development of *Heterodera glycines* in soybean roots and related and related anatomical changes. Phytopathology 54: 79–88.

Endo, B. 1965. Histological responses of resistant and susceptible soybean varieties, and backcross progeny to entry development of *Heterodera glycines*. Phytopathology 55: 375–381.

Endo, B. 1971. Synthesis of nucleic acids at infection sites of soybean roots parasitized by *Heterodera glycines*. Phytopathology 61: 395–399.

Ewing, B., Hillier, L., Wendl, M.C. and Green, P. 1998. Base-calling of automated sequencer traces using phred. I. Accuracy assessment. Genome Res. 8: 175–185.

Gaskin, F. and Kress, Y. 1977. Zinc ion-induced assembly of tubulin. J. Biol. Chem. 252: 6918–6924.

Gheysen, G. and Fenoll, C. 2002. Gene expression in nematode feeding sites. Annu. Rev. Phytopathol. 40: 191–219.

Gipson, I. and Kim Riggs, K.S. R.D. 1971. An ultrastructural study of syncytium development in soybean roots infected with *Heterodera glycines*. Phytopathology 61: 347–353.

Green, J., Vain, P., Fearnehough, T., Worland, B., Snape, J.W. and Atkinson, H.J. 2002. Analysis of the expression patterns of the *Arabidopsis thaliana* tubulin-1 and *Zea mays* ubiquitin-1 promoters in rice plants in association with nematode infection. Physiol. Mol. Plant Pathol. 60: 197–205.

Guiltinan, M.J., Ma, D.-P., Barker, R.F., Bustos, M.M. Cyr, R.J. and Yadegari Fosket, R. D.E. 1987. The isolation, characterization and sequence of two divergent beta-tubulin genes from soybean (*Glycine max* L.). Plant Mol. Biol. 10: 171–184.

Iscove, N.N., Barbara, M., Gu, M., Gibson, M., Modi, C. and Winegarden, N. 2002. Representation is faithfully preserved in global cDNA amplified exponentially from sub-picogram quantities of mRNA. Nat. Biotechnol. 20: 940–943.

Isenberg, G., Bielser, W., Meier-Ruge, W. and Remy, E. 1976. Cell surgery by laser micro-dissection: a preparative method. J. Microsc. 107: 19–24.

Javot, H. and Maurel, C. 2002. The role of aquaporins in root water uptake. Ann Bot 90: 301–313.

Jones, M.G.K. and Northcote, D.H. 1972. Nematode-induced syncytium – a multinucleate transfer cell. J. Cell. Sci. 10: 789–809.

Kerk, N., Ceserani, T., Tausta, S.L., Sussex, I. and Nelson, T. 2003. Laser-capture microdissection of cells from plant tissues. Plant Physiol. 132: 27–35.

Khan, R., Alkharouf, N., Beard, H.S., MacDonald, M., Chouikha, C., Meyer, S., Grefenstette, J., Knap, H. and Matthews, B. 2004. Microarray analysis of gene expression in soybean roots susceptible to the soybean cyst nematode two days post invasion. J. Nematol. 36: 241–248.

Klink, V.P. and Wolniak, S.M. 2001. Centrin is necessary for the formation of the motile apparatus in spermatids of *Marsilea*. Mol. Biol. Cell 12: 761–776.

Larsson, H., Wallin, M. and Edstrom, A. 1976. Induction of a sheet polymer of tubulin by Zn^{2+}. Exp. Cell. Res. 100: 104–110.

Lee, Y.R., Giang, H.M. and Liu, B. 2001. A novel plant kinesin-related protein specifically associates with the phragmoplast organelles. Plant Cell 13: 2427–2439.

Livak, K.J. and Schmittgen, T.D. 2001. Analysis of relative gene expression data using real-time quantitative PCR and the 2(-Delta Delta C(T)) method. Methods 25: 402–408.

Lloyd, C. and Chan, J. 2004. Microtubules and the shape of plants to come. Nat. Rev. Mol. Cell Biol. 5: 13–22.

Long, J.A. and Barton, M.K. 1998. The development of apical embryonic pattern in *Arabidopsis*. Development 125: 3027–3035.

Maitra, N. and Cushman, J.C. 1994. Isolation and characterization of a drought-induced soybean cDNA encoding a D95 family late-embryogenesis-abundant protein. Plant Physiol. 106: 805–806.

Marc, J., Granger, C.L., Brincat, J., Fisher, D.D., Kao, T.H., McCubbin, A.G. and Cyr, R.J. 1998. A GFP-MAP4 reporter gene for visualizing cortical microtubule rearrangements in living epidermal cells. Plant Cell 10: 1927–1940.

Matthews, B.F., Pilitt, K. and Klink, V. 2004. Molecular characterization of a soybean cyst nematode (*Heterodera glycines*) homolog of *unc-87*. J. Nematol. 36: 457–465.

Meimberg, H., Thalhammer, S., Brachmann, A., Muller, B., Eichacker, L.A., Heckl, W.M. and Heubl, G. 2003. Selection of chloroplasts by laser microbeam microdissection for single-chloroplast PCR. Biotechniques 34: 1238–1243.

Nakazono, M., Qiu, F., Borsuk, L.A. and Schnable, P.S. 2003. Laser-capture microdissection, a tool for the global analysis of gene expression in specific plant cell types: identification of genes expressed differentially in epidermal cells or vascular tissues of maize. Plant Cell. 15: 583–596.

Ramsay, K., Wang, Z. and Jones, M.G.K. 2004. Using laser capture microdissection to study gene expression in early stages of giant cells induced by root-knot nematodes. Mol. Plant Pathol. 5: 587–592.

Rao, S., Orr, G.A., Chaudhary, A.G., Kingston, D.G. and Horwitz, S.B. 1995. Characterization of the taxol binding site on the microtubule. 2-(m-Azidobenzoyl)taxol photolabels a peptide (amino acids 217–231) of beta-tubulin. J. Biol. Chem. 270: 20235–20238.

Sakr, S., Alves, G., Morillon, R., Maurel, K., Decourteix, M., Guilliot, A., Fleurat-Lessard, P., Julien, J.L. and Chrispeels, M.J. 2003. Plasma membrane aquaporins are involved in winter embolism recovery in walnut tree. Plant Physiol. 133: 630–641.

Sass, J.E. 1958. Botanical Microtechnique. Iowa State College Press, Ames.

Sivaguru, M., Pike, S., Gassmann, W. and Baskin, T.I. 2003. Aluminum rapidly depolymerizes cortical microtubules and depolarizes the plasma membrane: evidence that these responses are mediated by a glutamate receptor. Plant Cell Physiol. 44: 667–75.

Suga, S., Imagawa, S. and Maeshima, M. 2001. Specificity of the accumulation of mRNAs and proteins of the plasma membrane and tonoplast aquaporins in radish organs. Planta 212: 294–304.

Sugimoto, K, Williamson, RE and Wasteneys, GO 2000. New techniques enable comparative analysis of microtubule orientation, wall texture, and growth rate in intact roots of *Arabidopsis*. Plant Physiol. 124: 1493–1506.

The Gene Ontology Consortium 2004. The Gene Ontology (GO) database and informatics resource. Nucleic Acids Res. 32: D258–D261.

Tonoike, H., Han, I.S., Jongewaard, I., Doyle, M., Guiltinan, M. and Fosket, D.E. 1994. Hypocotyl expression and light downregulation of the soybean tubulin gene, tubB1. Plant J. 5: 343–351.

Van der Eycken, W., de Almeida Engler, J., Inze, D., Van Montagu, M. and Gheysen, G. 1996. A molecular study of root-knot nematode-induced feeding sites. Plant J. 9: 45–54.

Vercauteren, I., Van Der Schueren, , Van Moneagu, M. and Gheysen, G. 2001. *Arabidopsis thaliana* genes expressed in the early compatible interaction with root-knot nematodes. Mol. Plant–Microbe Interact. 14: 288–299.

Wallin, M., Larsson, H. and Edstrom, A. 1977. Tubulin sulfhydryl groups and polymerization in vitro. Effects of di- and trivalent cations. Exp. Cell Res. 107: 219–225.

Wrather, J.A., Stienstra, W.C. and Koenning, S.R. 2001. Soybean disease loss estimates for the United States from 1996 to 1998. Can. J. Plant. Pathol. 23: 122–131.

Yuan, M., Shaw, P.J., Warn, R.M. and Lloyd, C.W. 1994. Dynamic reorientation of cortical microtubules, from transverse to longitudinal, in living plant cells. Proc. Natl. Acad. Sci. USA 91: 6050–6053.